Hindawi
Advances in Condensed Matter Physics
Volume 2022, Article ID 4709525, 14 pages
https://doi.org/10.1155/2022/4709525

Research Article

Oxygen Dependence of Formation, Electronic State Transition, and Spin Polarization for Anatase TiO_2: A Comprehensive Study

L. L. Shan,[1] R. M. Fan,[1] Y. Sun,[2] F. P. Zhang,[2,3,4] G. L. Zhang,[3,4] and G. Q. Qin[4]

[1]*Henan Provincial Key Laboratory of Biological Psychiatry, Department of Biochemistry and Molecular Biology, School of Basic Medical Sciences, Xinxiang Medical University, 453003 Xinxiang, China*
[2]*Department of Physics, Changji University, Changji 831100, China*
[3]*Henan Provincial Engineering Laboratory of Building-Photovoltaics, Institute of Physics, Henan University of Urban Construction, Pingdingshan, Henan 467036, China*
[4]*School of Materials Sciences and Engineering, Shijiazhuang Tiedao University, Shijiazhuang 050043, China*

Correspondence should be addressed to Y. Sun; sunyi@cjc.edu.cn and F. P. Zhang; zhfp@emails.bjut.edu.cn

Received 13 September 2021; Accepted 21 March 2022; Published 11 April 2022

Academic Editor: Ashwini Kumar

Copyright © 2022 L. L. Shan et al. This is an open access article distributed under the Creative Commons Attribution License, which permits unrestricted use, distribution, and reproduction in any medium, provided the original work is properly cited.

The stability, geometry, microstructure, and specie combination together with the electronic states of the anatase TiO_2 with oxygen defect content of 0%, 3.125%, 6.25%, and 12.5% have been intensively studied within the framework of the density functional theory method. The results show that the TiO_2 with an oxygen defect is not as stable as intrinsic TiO_2. The compound formation enthalpy E_f and the oxygen defect formation energy value tend to be larger for a higher defect content, and the oxygen defect gets harder to be formed. The bonds within the TiO_6 polyhedron are different and not geometrically symmetrical. The bond strengths show distinct diversity, and the primitive cell of anatase TiO_2 show spatial expansion when there are oxygen defects. All bands moved down to the low energy region, and two impurity energy band levels emerged for the anatase TiO_2 with oxygen defect. The energy band gap is decreased from 3.085 eV to 1.165 eV, 1.0015 eV, and 0.43 eV. There are generally 7 peaks for the spin density of states function, corresponding to their 5 main bands. For the anatase TiO_2 with an oxygen defect content of 12.5%, the spin density of states functions are not horizontal ordinate symmetrical near −1.12 eV and 0.31 eV. They are formed by oxygen defect energy levels, which is the result of the Ti d and O p state electron polarization. Transitions from weak paramagnetic to antiferromagnetic are found for the anatase TiO_2 with oxygen defect.

1. Introduction

Titanium dioxide (TiO_2) is a kind of environmentally friendly material, and it has advantages such as chemical stability, easy fabrication, nontoxic release, and cheap raw material. TiO_2 matrix materials can be applied widely in fields such as coatings, rubbers, fibers, cosmetics, functional building materials, and modern electronic industries [1–5]. In general, the TiO_2 matrix materials can be prepared experimentally by the hydrothermal method, sol-gel method, and solid-state reaction method, and the method described by Anh et al. [3]. Various defects can be generated inevitably, and the TiO_2 matrix materials should be modulated in terms of their geometric structure, physical properties, and performance. The defect can usually be introduced naturally during the material preparation process, for example, intrinsic defects, such as titanium vacancy, oxygen vacancy, titanium site substitution by oxygen, oxygen site substitution by titanium, and Frenkel defect as well as exotic doping defect [6]. The electronic states can then be tailored thereafter. For instance, the band gap should be modulated, defect levels should be induced, the transition mechanism of carriers should be modified, the band configurations should also be tailored, and the carrier mobility, concentration, and generation-combination mechanic details can also be modulated. The defect can be introduced manually in the

preparation process, too. The effects of exotic dopant on TiO_2 have been widely investigated previously, for example, the main group elements, that is, nitrogen, lithium, sulfur, boron, carbon, phosphorus, etc., and the transitional group elements, that is, cobalt, zinc, manganese, ferrous, vanadium, etc. Additionally, there are noble metal elements, that is, gold, silver, ruthenium, etc. The multimagnetism phases have also been revealed for the doped TiO_2 [3–11]. The variety of physical properties as well as the performances is very reach, and they merit valuable investigation.

TiO_2 exhibits three types of crystal structures, namely, the anatase phase, rutile phase, and brookite phase. Among these three phases, the anatase-phase TiO_2 is the most stable at ordinary temperature and there are more reports on this [3–5]. Figure 1 shows the geometrical structure of the anatase-phase TiO_2 framework. It exhibits a tetragonal structure with high geometric symmetry. Ti forms polyhedron with six neighbouring O and locates within the polyhedron. O forms tetrahedron with three neighboring Ti and locates within the tetrahedron. The intrinsic defects are very important and meaningful for TiO_2, they can be generated inevitably in the preparation process, and it is valuable to investigate the effect of the intrinsic defect on stability and geometry as well as the electronic states for anatase TiO_2. Specifically, the oxygen defect can be easily introduced than titanium within the material preparation procedure as a result of oxygen pressure variation. In this study, the effects of intrinsic oxygen defect at different contents on stability, geometry evolution, specie combination, and electronic states, as well as the magnetic property for the anatase TiO_2 have been systematically investigated within the framework of the density functional theory calculational and analyzing method.

2. Models and Computational Details

The anatase-phase TiO_2 is composed of titanium sublattice and the oxygen sublattice, and it has a tetragonal geometric structure with a space group of $I4_1/amd$. The titanium is surrounded by six oxygen within the anatase-phase TiO_2 geometric structure, and every oxygen is linked by three titaniums. For the primitive cell, the angle constants α, β, and γ are 90°. The axial length constants a, b, and c are 3.776 Å, 3.776 Å, and 9.486 Å, respectively [2–4]. Figure 1 shows the schematical picture of crystal geometry and basis vector direction for anatase TiO_2 in which the red sphere represents oxygen and the gray sphere represents titanium. Figure 2 shows specifically the projections on to (100) plane, (010) plane, and (001) plane for anatase TiO_2 to further guide the eyes. In this study, the primitive cell models with formulas of $Ti_{16}O_{31}$, Ti_8O_{15}, Ti_4O_7, and Ti_4O_8 were established, which correspond to oxygen defect contents of 3.125%, 6.25%, 12.5%, and 0%, respectively.

The density functional theory (DFT) method has been demonstrated to be one of the most accurate strategies for the deductions and solutions of the electronic eigenvalues of condensed matters [12–15]. This study was carried out based on the platform that is implemented in the Serial Total Energy Package (CASTEP, Cerius2, Molecular Simulation,

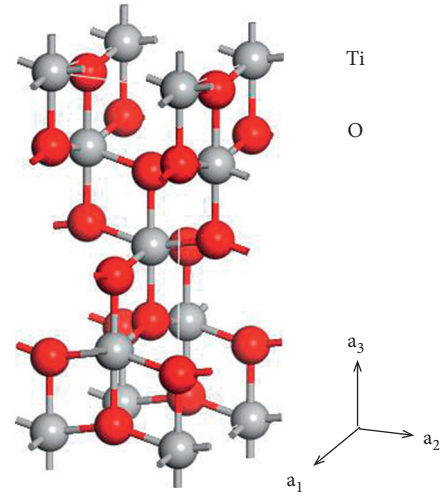

Figure 1: Schematical picture of crystal geometry and basis vector direction for anatase TiO_2 in which the red sphere represents oxygen and the gray sphere represents titanium.

Inc.) code within the framework of the DFT [12, 14]. This coded package is established within the framework of the DFT, which has been successfully applied in the fields such as solid states, material sciences, biological sciences, and quantum chemistries for several years [12–15]. In this study, the atomic core and the inner valance electrons were treated as Coulombic cores, and the Coulomb interactions of cores with their outer valance electrons were described by Vanderbilt pseudo-potentials functions. The wave functions of these electrons were represented by plane wave functions. The configurations of pseudovalence electrons for Ti and O were selected as $Ti(3s^23p^63d^24s^2)$ and $O(2s^22p^4)$, respectively. The generalized gradient approximation (GGA) scheme and revised Perdew–Burke–Ernzerhof (RPBE) function within the scheme were adopted to describe the exchange-correlation relation effect among these electrons. Ti has d state electrons, and the Hubbard energy revision of 2.5 eV was used to describe the on-site Coulomb effect; it has been verified to be enough for description and expansion of the band levels. In this study, Ti d orbital anti-ferromagnetic-aligned TiO_2 has been set and the paramagnetic phase has been verified to be more thermally stable. The convergence tolerance of displacement within the self-consistent calculations was set as 0.001 Å, and the maximum force tolerance was set as 5×10^{-6} eV/atom in the ground state total energy calculation. The cutoff energy for electron plane wave expansion of the wave functions was set as 260 eV. For the k point sampling, the Monkhorst–Pack method was used and the k point grid is $1 \times 1 \times 1$. In this study, the resolution of the Schrödinger equation was carried out within the reciprocal space of wave vector sampling for TiO_2 lattice, and the origins of coordinates are the same in terms of the two spaces. The electron eigenvalues are deduced, and the plane wave function set are expanded within the first Brillouin zone as a function of high symmetry points. The reduced Brillouin zone for the anatase TiO_2 structure and the coordinates of irreducible high symmetry points are shown in Figure 3 and Table 1, respectively.

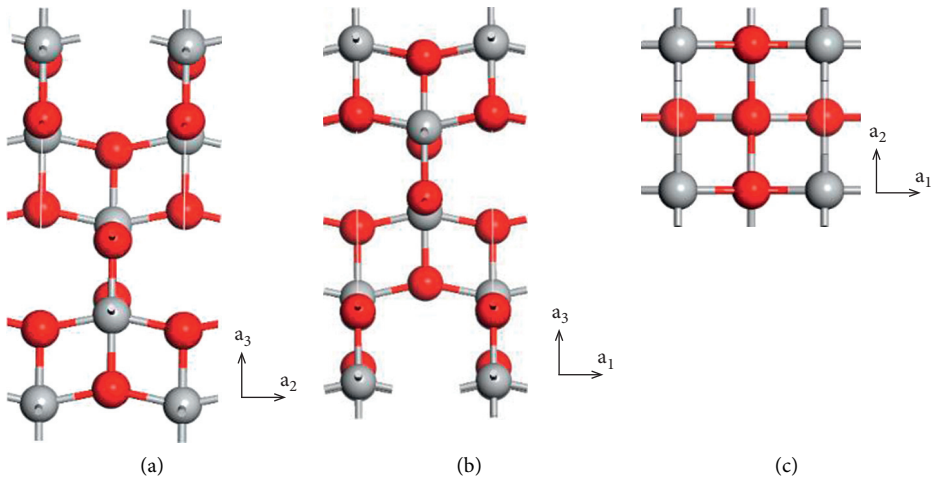

Figure 2: Projections on to (100) plane (a), (010) plane (b), and (001) plane (c) for anatase TiO_2 in which the red sphere represents oxygen and the gray sphere represents titanium.

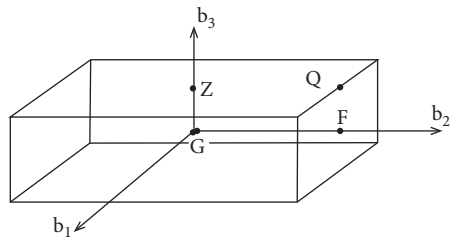

Figure 3: The reduced Brillouin zone for anatase TiO_2 in which the G point is the origin of coordinate.

Table 1: Coordinates of high symmetry points within the first Brillouin zone for anatase TiO_2.

G	F	Q	Z
0, 0, 0	0, 0.5, 0	0, 0.5, 0.5	0, 0, 0.5

3. Results and Discussion

3.1. Stability. The total energy of the modeled system can be applied for analyzing the thermal stability of materials. Table 2 shows the normalized total energies E_t for the systems with oxygen defect content of 0%, 3.125%, 6.25%, and 12.5%. It can be seen that the system with an oxygen defect content of 0% has a total energy of −39642.2764 eV; note that it is also a value for the intrinsic TiO_2. The system with an oxygen defect content of 3.125% has a total energy of −39203.8242 eV, which is 420.4522 eV higher than that of intrinsic TiO_2. It is indicated that the oxygen-defected TiO_2 is not as stable as the intrinsic TiO_2, and excessive energy should be needed in order to form the oxygen defect within the anatase TiO_2. It can be seen that the systems with oxygen defect contents of 6.25% and 12.5% have total energies of −38765.2953 eV and −37887.9081 eV, which are 876.9811 eV and 1754.3683 eV higher than that of the intrinsic TiO_2. It is further suggested that the oxygen-defected TiO_2 systems are all not as stable as the intrinsic TiO_2. Secondly, it can be obviously observed that the total energy is enlarged along with the increasing oxygen defect content. It is true that the oxygen defect within the anatase TiO_2 is increasingly hard to form within the present study. Thirdly, it can be deduced that the excessive energy for oxygen defect formation is not linearly dependent on its content. Figure 4 shows the normalized total energy increment for oxygen-defected TiO_2 at a content of 3.125%. It can be seen that excessive energy of 420.4522 eV, 438.4905 eV, and 438.5921 eV should be needed for oxygen defect formation. It gets harder for the oxygen defect to form within the study region. For example, energy of 420.4522 eV is needed for oxygen defect formation with a content of 3.125%, energy of 438.4905 eV is needed for oxygen defect formation with another content of 3.125%, and energy of 438.5921 eV is needed for oxygen defect formation with still another content of 3.125%. The oxygen defect is harder to form by increasing its content, and the TiO_2 system is more thermally stable at a lower oxygen defect content.

Table 2: Normalized total energy E_t, formation enthalpy E_f, oxygen defect formation energy E_d, and magnetism for anatase TiO_2.

O content/%	E_t/eV	E_f/eV	E_d/eV	Magnetism
0	−39642.2764	−7.5122	—	PM
3.125	−39203.8242	−7.4788	10.6721	AFM
6.25	−38765.2953	−7.1619	10.7105	AFM
12.5	−37887.9081	−6.8003	10.8121	AFM

In order to further evaluate the thermal stability of oxygen-defected anatase TiO_2 materials at different contents, the formation enthalpy is adopted. The formation enthalpy is enthalpy change for the formation of 1 mol of a compound from its component elements, and compounds with smaller formation enthalpy should be more thermally stable. The formation enthalpy E_f for a kind of compound xAyB can be formulated by

$$E_f = \frac{E_t - x\mu_A - y\mu_B}{x + y}, \quad (1)$$

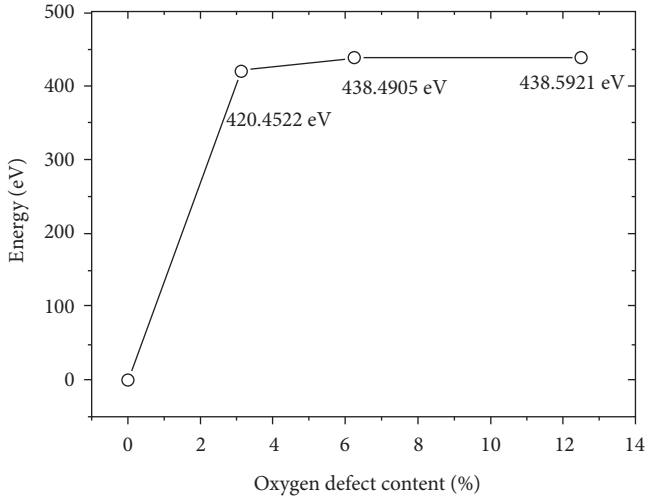

Figure 4: Normalized total energy increment for oxygen-defected TiO_2 as a function of content.

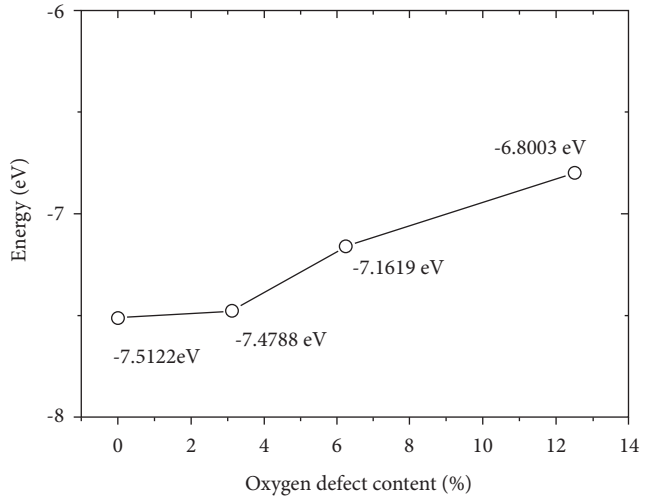

Figure 5: Normalized formation enthalpy E_f for the TiO_2 system as a function of oxygen defect content.

where μ_A and μ_B are the chemical potentials of elements A and B. The E_t is the total energy of the compound [14, 16, 17]. Table 2 shows the normalized formation enthalpy E_f for the systems with oxygen defect contents of 0%, 3.125%, 6.25%, and 12.5%. It is seen that the formation enthalpies E_f for the systems is −7.5122 eV, −7.4788 eV, −7.1619 eV, and −6.8003 eV, respectively. It is worth noting that the formation enthalpy E_f is dependent on the oxygen defect content, and it is increased by increasing the oxygen defect content. For instance, the formation enthalpy for the intrinsic TiO_2 is −7.5122 eV, it is increased to −7.4788 eV for the system with an oxygen defect content of 3.125%, and it is still increased to −7.1619 eV for the system with an oxygen defect content of 6.25%, and the system with the highest oxygen defect content of 12.5% has the largest formation enthalpy of −6.8003 eV. The compound with the most oxygen defect has the largest formation enthalpy; it is hardest to be formed. This is in good accordance with the total energy. Furthermore, Figure 5 shows the normalized formation enthalpy E_f for the systems as a function of oxygen defect content. It can be observed that the formation enthalpy E_f is not linearly dependent on the defect content. In other words, the formation enthalpy E_f value is not proportional to the oxygen defect content, and it tends to be larger with the increasing content. It is an indication that the oxygen defect gets harder to be formed. This is in agreement with the total energy.

In order to evaluate the energy order of magnitude and formation capability of the oxygen defect within anatase TiO_2, the formation energy of oxygen defect is deduced. The formation energy of oxygen defect E_d can be formulated by

$$E_d = E_{td} - E_{ti} + \mu_d - \mu_i, \quad (2)$$

where E_{td} and E_{ti} are the total energies of oxygen defected systems and intrinsic system, respectively [12, 18]. μ_v and μ_i are the chemical potential of the defect and oxygen, respectively [12, 19, 20]. Table 2 shows the normalized oxygen defect formation energy E_d for the systems with oxygen defect contents of 3.125%, 6.25%, and 12.5%. It can be seen that the order of magnitude for oxygen defect formation energy is approximately 10 eV. Moreover, the oxygen defect formation energy value tends to be larger for a higher defect content. This is consistent with the total energy and formation enthalpy. Figure 6 shows the normalized oxygen defect formation energy E_d for the system as a function of content. It is the same consequence that the oxygen defect formation energy E_d is not linearly dependent on the defect content. The oxygen defect formation energy E_d value is not proportional to the oxygen defect content, and it tends to be larger with the increasing content. It is once again evidenced that the oxygen defect gets harder to be formed.

3.2. Geometry. Table 3 shows the normalized lattice parameters for intrinsic anatase TiO_2 and oxygen-defected anatase TiO_2 with content of 3.125%, 6.25%, and 12.5%, respectively. The italic data represent the experimental values for the intrinsic anatase TiO_2. L is the sum of a, b, and c. Figure 7 shows the lattice constants for anatase TiO_2 as a function of oxygen defect content. The deviations of obtained lattice constants from experimental values are no more than 1%, and the calculational results can be regarded as reasonable. It can be seen from Table 3 and Figure 7 that the lattice constants are changed. The a is firstly decreased and then increased, and its values for oxygen-defected systems are all smaller than those for the intrinsic system. The fluctuation of b shows the same trend as that of a; however, its values for oxygen-defected systems (with contents of 6.25% and 12.5%) get larger than those for the intrinsic system. The fluctuation of c shows the reverse trend as that of a and b, and its values for oxygen-defected systems are all larger than those for the intrinsic system. L exhibits the same trend and phenomenon as that of c. It can be seen that the primitive cell of anatase TiO_2 shows spatial expansion when oxygen defect occurs. It is deduced that strain and stress should be induced for the anatase TiO_2 with oxygen defect, compressive stress should be produced along

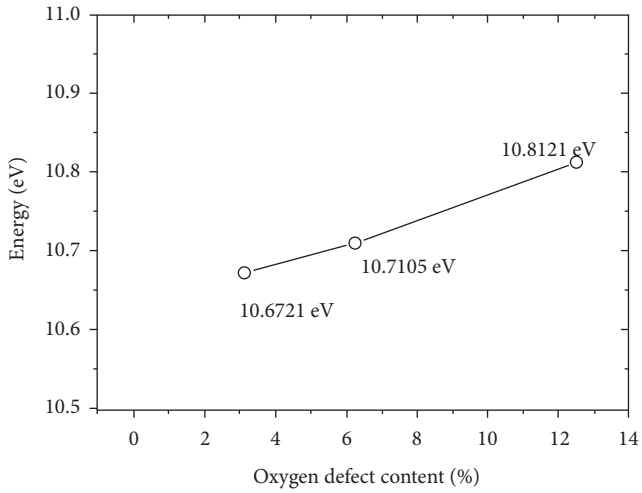

Figure 6: Normalized oxygen defect formation energy E_d for the TiO_2 system as a function of content.

Table 3: Lattice constants for intrinsic anatase TiO_2 and oxygen-defected anatase TiO_2.

O Content/%	a/Å	b/Å	c/Å	L/Å	α/°	β/°	γ/°
0	3.776 3.810	3.776 3.810	9.486 9.664	17.038 17.284	90	90	90
3.125	3.764	3.762	9.952	17.478	90.04	90.03	90.02
6.25	3.773	3.819	9.721	17.313	90	90	90
12.5	3.787	3.832	9.684	17.303	89.98	90.25	89.99

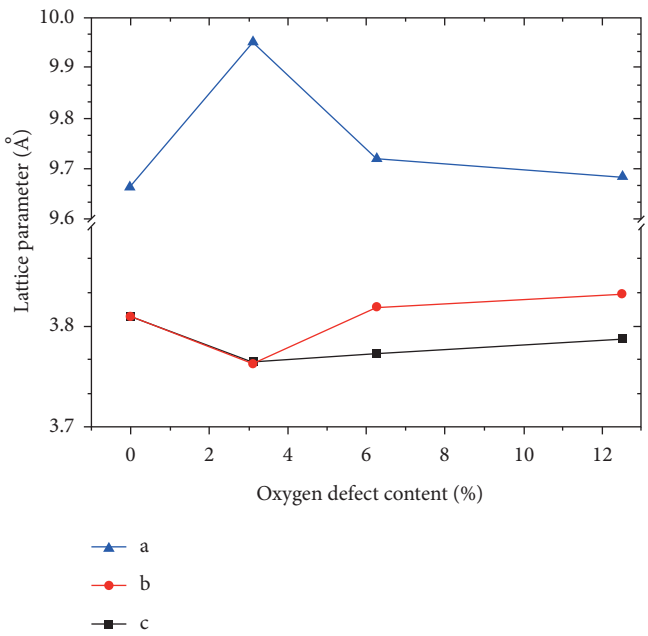

Figure 7: Lattice constants for anatase TiO_2 as a function of oxygen defect content.

a direction within the whole studying region, and compressive stress and tensile stress should be produced along b and c direction, respectively, at a lower oxygen defect content [20, 21].

The tetragonal anatase TiO_2 framework is constructed by TiO_6 polyhedron in which one titanium is surrounded by six oxygen and one oxygen is linked by three Titaniums. Figure 8 shows the TiO_6 polyhedron within the geometric framework of anatase TiO_2. Table 4 shows the bond length b_{li} of Ti-O for intrinsic anatase TiO_2 and oxygen-defected anatase TiO_2. The four bond lengths represent the bonds parallel to the a-b plane (a_1-a_2 plane), and the two bond lengths represent the bonds parallel to the c direction (a_3 direction). It can be observed that the bonds within the polyhedron are different for the intrinsic TiO_2, which demonstrates that the polyhedron is not geometrically symmetrical. It can be seen that the bond lengths parallel to the a direction (b_{l1} and b_{l2}) exhibit firstly a decreasing and then increasing trend, in accordance with the primitive cell constant fluctuations. The bond lengths parallel to the b direction (b_{l3} and b_{l4}) exhibit the same trend as that of a, which is in accordance with the primitive cell constant fluctuations. The bond lengths parallel to the c direction (b_{l5} and b_{l5}) exhibit the reverse trend; for example, the bond length b_{l6} is firstly increased and then decreased, and its values for oxygen-defected systems are all larger than those for the intrinsic system. This is in good agreement with the lattice constant fluctuations.

3.3. Specie Combination. Table 4 shows the bond strength of Ti-O for intrinsic anatase TiO_2 and oxygen-defected anatase TiO_2. The number of zero represents the totally ionic bond and Coulomb interaction between species. The number of unit represents the totally covalent bond between species. It can be seen that the bonds parallel to a and b directions (b_{l1}, b_{l2}, b_{l3}, and b_{l4}) have a larger bond strength value of 0.69, and the bonds parallel to the c direction (b_{l5} and b_{l5}) have a smaller bond strength value of 0.29 for the intrinsic TiO_2. These suggest their strong covalent bonds and weak covalent bonds, respectively. This is the same phenomenon for all TiO_2 systems in this study. In addition, generally speaking, when there are oxygen defects, the strong covalent bonds parallel to a and b directions (b_{l1}, b_{l2}, b_{l3}, and b_{l4}) show decreased bond strength values, and the weak covalent bonds parallel to c direction (b_{l5} and b_{l5}) show increased bond strength values. For example, the bond strength values of b_{l1}, b_{l2}, b_{l3}, and b_{l4} decreased to be 0.44, 0.42, 0.41, and 0.37 for the TiO_2 with an oxygen defect content of 3.125%. Secondly, when there are oxygen defects, the bond strengths within the polyhedron show distinct diversity. Some bonds are strengthened, and some bonds are weakened; this phenomenon could be considered electron redistribution among their cores with resulting bond effect modulations [22].

3.4. Electronic States. Figure 9 shows the full energy range band structures for anatase TiO_2 with oxygen defect contents of 0%, 3.125%, 6.25%, and 12.5%. The Fermi energy is set as zero, and other energy levels are set relatively compared to Fermi energy [23]. As is shown in Figure 9, there are five bands for intrinsic anatase TiO_2, which locates near 2.5 eV~5 eV, −4 eV~0 eV, −17.5 eV ~ −16 eV, −33 eV, and

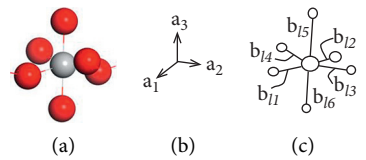

Figure 8: The TiO_6 polyhedron within the geometric structure of anatase TiO_2 in which the red sphere represents oxygen and the gray sphere represents titanium (a), basis vector direction, (b) and schematic geometry and bond marks of the polyhedron (c).

Table 4: Bond length for b_{li} and bond strength of Ti-O for intrinsic anatase TiO_2 and oxygen-defected anatase TiO_2.

O content/%	Bond length for b_{li}/Å $b_{l1}/b_{l2}/b_{l3}/b_{l4}$ B_{l5}/b_{l6}	Bond strength
0	1.952/1.953/1.953/1.954	0.69
	1.984/1.989	0.29
3.125	1.886/1.889/1.903/1.958	0.44/0.42/0.41/0.37
	1.891/2.033	0.34/0.23
6.25	1.898/1.899/1.928/1.938	0.75/0.43/0.43/0.39
	1.910/2.019	0.37/0.2
12.5	1.932/1.934/1.941/1.950	0.72/0.72/0.69/0.29
	1.977/2.002	0.28/0.27

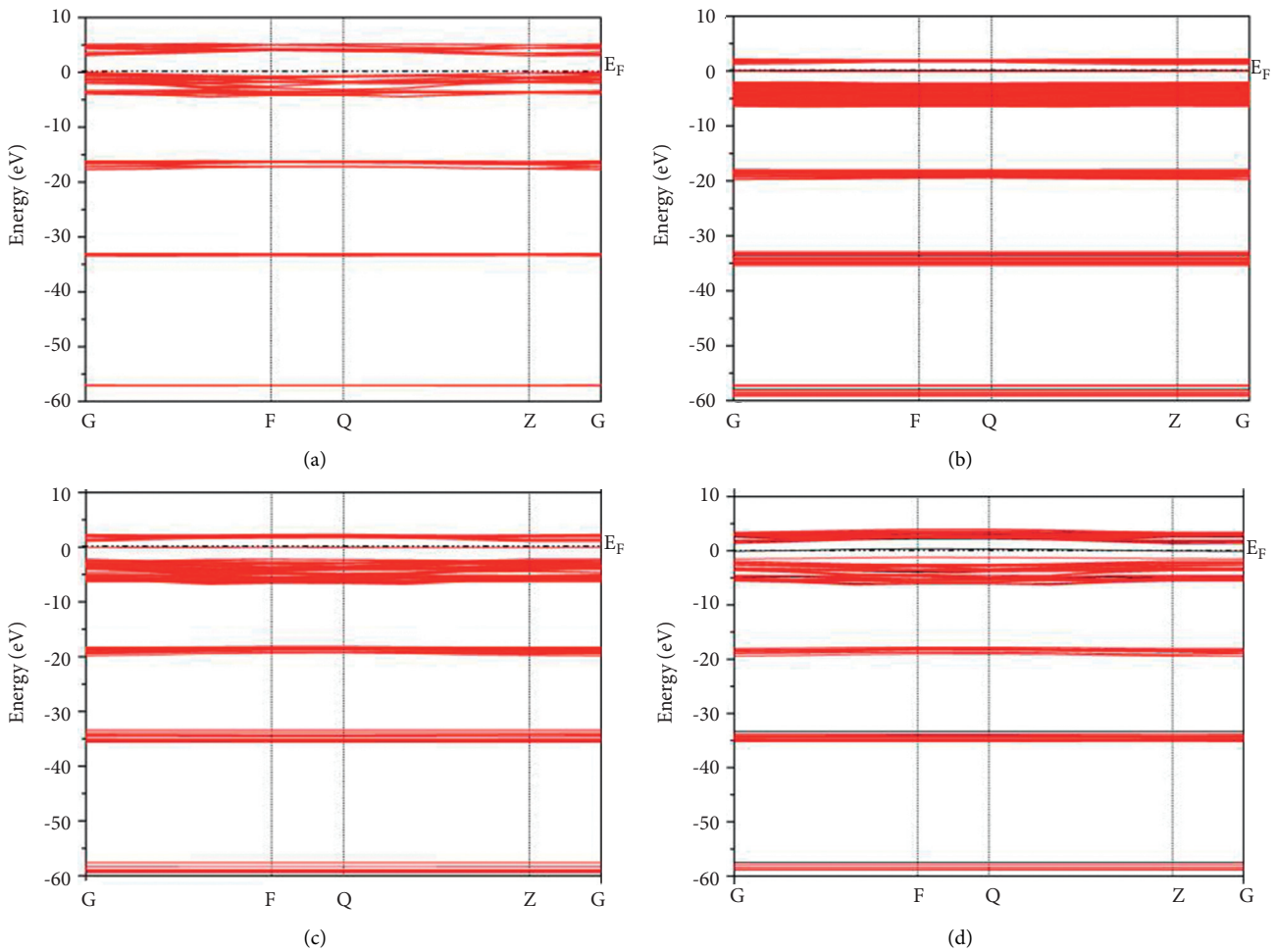

Figure 9: Full energy range band structure for anatase TiO_2 with oxygen defect contents of 0% (a), 3.125% (b), 6.25% (c), and 12.5% (d).

−57 eV. The first valance band and the conduction band show more wide energy distribution. There are five main bands for anatase TiO_2 with oxygen defect contents of 3.125%, 6.25%, and 12.5%. It is observed that all bands moved down to the low energy region. The conduction band is narrowed, while the valance bands are widened. It can also be seen that impurity energy band levels emerged for the anatase TiO_2 with oxygen defect.

Figure 10 shows the band structures near Fermi energy for anatase TiO_2 with oxygen defect contents of 0%, 3.125%, 6.25%, and 12.5%. As is shown in Figure 10, the Fermi energy locates at the same level as that of the first upper valance band level. The first lower conduction band locates at 3.085 eV above Fermi energy. The energy valley and peak locates at different points, and an indirect energy gap of 3.085 eV is found for the intrinsic TiO_2. The intrinsic TiO_2 belongs to a semiconductor. This is well consistent with former reports [5–8]. For the anatase TiO_2 with oxygen defect, the conduction band and first valance band move downwards at the same time. For instance, the lowest level of the conduction band moves to 1.253 eV above Fermi energy and the first level of the upper valance band moves to −2.057 eV below Fermi energy for anatase TiO_2 with an oxygen defect content of 3.125%. The gap between them is 3.310 eV, which is larger than that of the intrinsic anatase TiO_2. The lowest level of the conduction band moves to 1.007 eV above Fermi energy, and the first level of the upper valance band moves to −2.185 eV below Fermi energy for anatase TiO_2 with an oxygen defect content of 6.25%. The gap between them is 3.192 eV, which is also larger than that of the intrinsic anatase TiO_2. For anatase TiO_2 with an oxygen defect content of 12.5%, the lowest level of the conduction band moves to 1.304 eV above Fermi energy and the first level of the upper valance band moves to −1.932 eV below Fermi energy. The gap between them is 3.236 eV, which is also larger than that of the intrinsic anatase TiO_2. The energy valley and peak locates at different points, and the anatase TiO_2 with oxygen defect belongs to the semiconductor, too. On the other hand, two defect levels can be found for the anatase TiO_2 with oxygen defect. Table 5 shows the collected band gaps, band gap type, and the number of defect bands for anatase TiO_2 with various contents of oxygen defect. There are two defect levels for all anatase TiO_2 with various contents of oxygen defect. The energy gap is divided by these defect levels into several subgaps. There are 2, 2, and 3 subgaps for the anatase TiO_2 with oxygen defect contents of 3.125%, 6.25%, and 12.5%, respectively. Energy potential for carrier to transit is decreased. Secondly, the energy gap among the subgaps is decreased along with the increasing content of the oxygen defect. For example, the energy gap is 1.165 eV and 2.019 eV for the anatase TiO_2 with an oxygen defect content of 3.125%. The energy gap is 1.0015 eV and 2.17 eV for the anatase TiO_2 with an oxygen defect content of 6.25%. Moreover, the three energy gaps are 0.928 eV, 1.147 eV, and 0.43 eV for the anatase TiO_2 with an oxygen defect content of 12.5%. The narrowest energy gap is decreased from 3.085 eV to 1.165 eV, 1.0015 eV, and 0.43 eV. It can be evidenced that energy potential for carrier to transit is indeed reduced. However, it can be inferred that the carrier recombination among energy levels should be facilitated and it gets easier. Thirdly, the two defect energy levels locate both near Fermi energy for anatase TiO_2 with oxygen defect contents of 3.125% and 6.25%, respectively. And the spin polarization of them can be regarded as negligible. Nevertheless, the two defect energy levels locate near Fermi energy at distinctly different energy regions for anatase TiO_2 with an oxygen defect content of 12.5%, and a local spin polarization of these two bands can be speculated.

Figure 11 shows the full energy range spin density of states for anatase TiO_2 with oxygen defect contents of 0%, 3.125%, 6.25%, and 12.5%. There are totally 7 peaks for the spin density of state curve for the intrinsic TiO_2, corresponding to its 5 bands. For the anatase TiO_2 with oxygen defect contents of 3.125%, 6.25%, and 12.5%, there are emerging peaks found as a result of oxygen defect levels. For the anatase TiO_2 with oxygen defect contents of 3.125% and 6.25%, the spin density of states curves are all horizontal ordinate symmetrical, and no visible spin polarization can be detected. However, for the anatase TiO_2 with an oxygen defect content of 12.5%, the spin density of state curves is not horizontal ordinate symmetrical, and obvious spin polarization can be detected. For example, four obvious nonhorizontal ordinate symmetries can be observed at −57.53 eV, −33.84 eV, −1.12 eV, and 0.31 eV. Local spin polarization of density of state can be demonstrated.

Figure 12 shows the spin density of states near Fermi energy for anatase TiO_2 with oxygen defect contents of 0%, 3.125%, 6.25%, and 12.5%, respectively. There are generally 4 peaks for the spin density of states curve for the intrinsic TiO_2, corresponding to its 2 bands near Fermi energy. This is the same phenomenon for the anatase TiO_2 with oxygen defect. For the anatase TiO_2 with oxygen defect contents of 3.125%, 6.25%, and 12.5%, there are excessive peaks between the gap found as a result of oxygen defect levels. For the anatase TiO_2 with oxygen defect contents of 3.125% and 6.25%, the spin density of state curves is all horizontal ordinate symmetrical, and no visible spin polarization can be detected in this energy area. For the anatase TiO_2 with an oxygen defect content of 12.5%, the spin density of states curves are distinctively not horizontal ordinate symmetrical, and obvious local spin polarization can be detected at −1.12 eV and 0.31 eV within this energy region. Local spin polarization of density of state can be obviously demonstrated. In addition, the nonhorizontal ordinate symmetry can be deduced to be formed by oxygen defect energy levels.

Figure 13 shows the spin density of states near the Fermi level of Ti for anatase TiO_2 with oxygen defect contents of 0%, 3.125%, 6.25%, and 12.5%,. There is a peak at 4.1 eV for the spin density of state curve for the intrinsic TiO_2, corresponding to its d state electron concentration at this energy area, and this also indicates its localization effect at this energy area. Within the upper valance band area, there is a wide distribution of the spin density of state curve and no steep peak found. This is the same for Ti within all the anatase TiO_2. It can be seen that the energy area (4.1 eV) that the peak within the conduction band locates is decreased to 1.8 eV, 1.9 eV, and 2.5 eV, which correspond to the movement of the conduction band to lower energy area. As can be

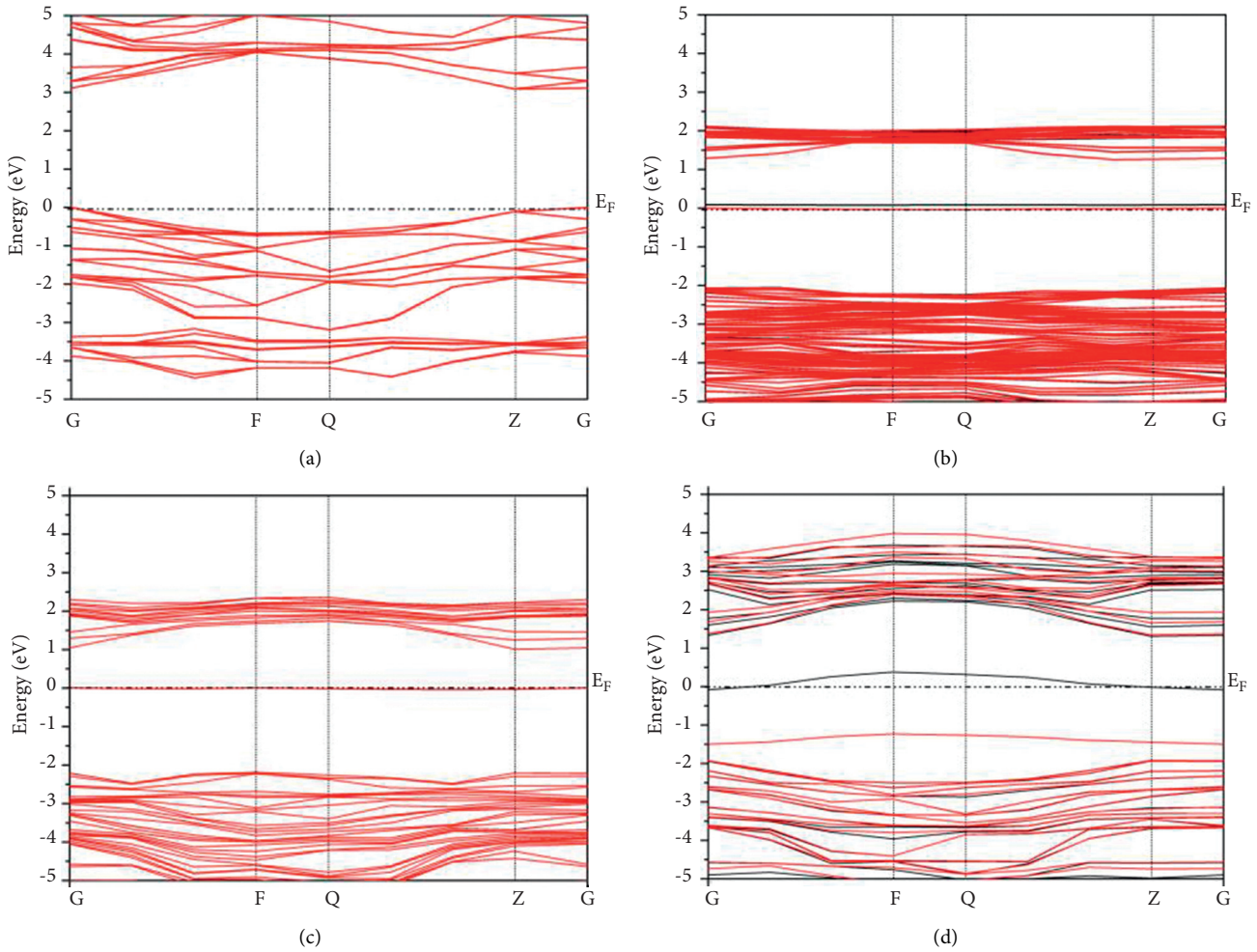

Figure 10: Band structure near the Fermi level for anatase TiO_2 with oxygen defect contents of 0% (a), 3.125% (b), 6.25% (c), and 12.5% (d).

Table 5: Band gaps, band gap type, and the number of defect band for anatase TiO_2.

O content/%	Band gap/eV	Band gap type	Defect band number
0	3.085	Indirect	0
	1.165 up gap	Indirect	
3.125	2.019 down gap	Indirect	2
	1.0015 up gap	indirect	
6.25	2.17 down gap	Indirect	2
	0.928 up gap	indirect	
12.5	1.147 middle gap	Indirect	2
	0.43 down gap	Indirect	

seen that the width of density of state curve of the conduction band area is also decreased, which corresponds to its electron concentration localization effect in this energy area, too. Furthermore, it can be seen that the anatase TiO_2 with oxygen defect contents of 0%, 3.125%, and 6.25%, the spin density of states curves of Ti are all horizontal ordinate symmetrical, and no apparently obvious spin polarization can be detected. The anatase TiO_2 with an oxygen defect content of 12.5% is found without horizontal ordinate symmetry for the spin density of states curve near Fermi energy, and there are two nonhorizontal ordinate symmetry peaks found at −1.1 eV and 0.2 eV. They are formed by the oxygen defect levels as shown in Figure 13(d). The local spin polarization can be inferred, and this is the result of the Ti d state electron polarization in these areas. No visible polarization is found for the Ti s and Ti p state electrons. It is true that the Ti d state electrons should be responsible for the local spin polarization for the anatase TiO_2 with an oxygen defect content of 12.5%.

Figure 14 shows the spin density of states near the Fermi level of O for anatase TiO_2 with oxygen defect contents of 0%, 3.125%, 6.25%, and 12.5%. There are several peaks under

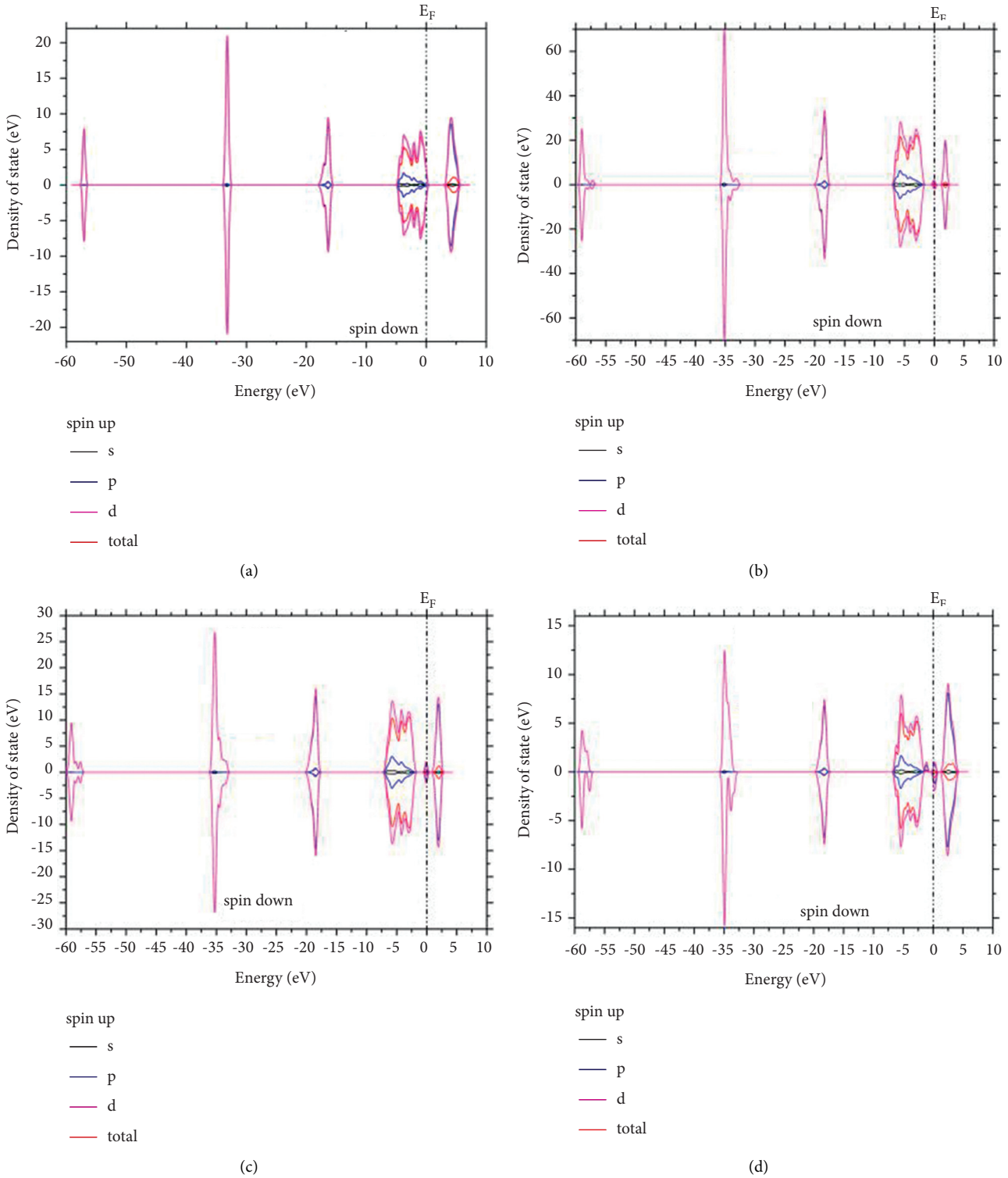

Figure 11: Full energy range spin density of states for anatase TiO_2 with oxygen defect contents of 0% (a), 3.125% (b), 6.25% (c), and 12.5% (d).

Fermi energy for the spin density of states curve for the intrinsic TiO_2, and the density of states curve values are higher than that of the density of states curve values above Fermi energy. The O state electrons form the upper valance band. This is the same for O within all the anatase TiO_2. It can be seen that for the anatase TiO_2 with oxygen defect contents of 0%, 3.125%, and 6.25%, the spin density of states curves of O are all horizontal ordinate symmetrical, and no spin polarization can be detected. It is worth noting that the anatase TiO_2 with an oxygen defect content of 12.5% is

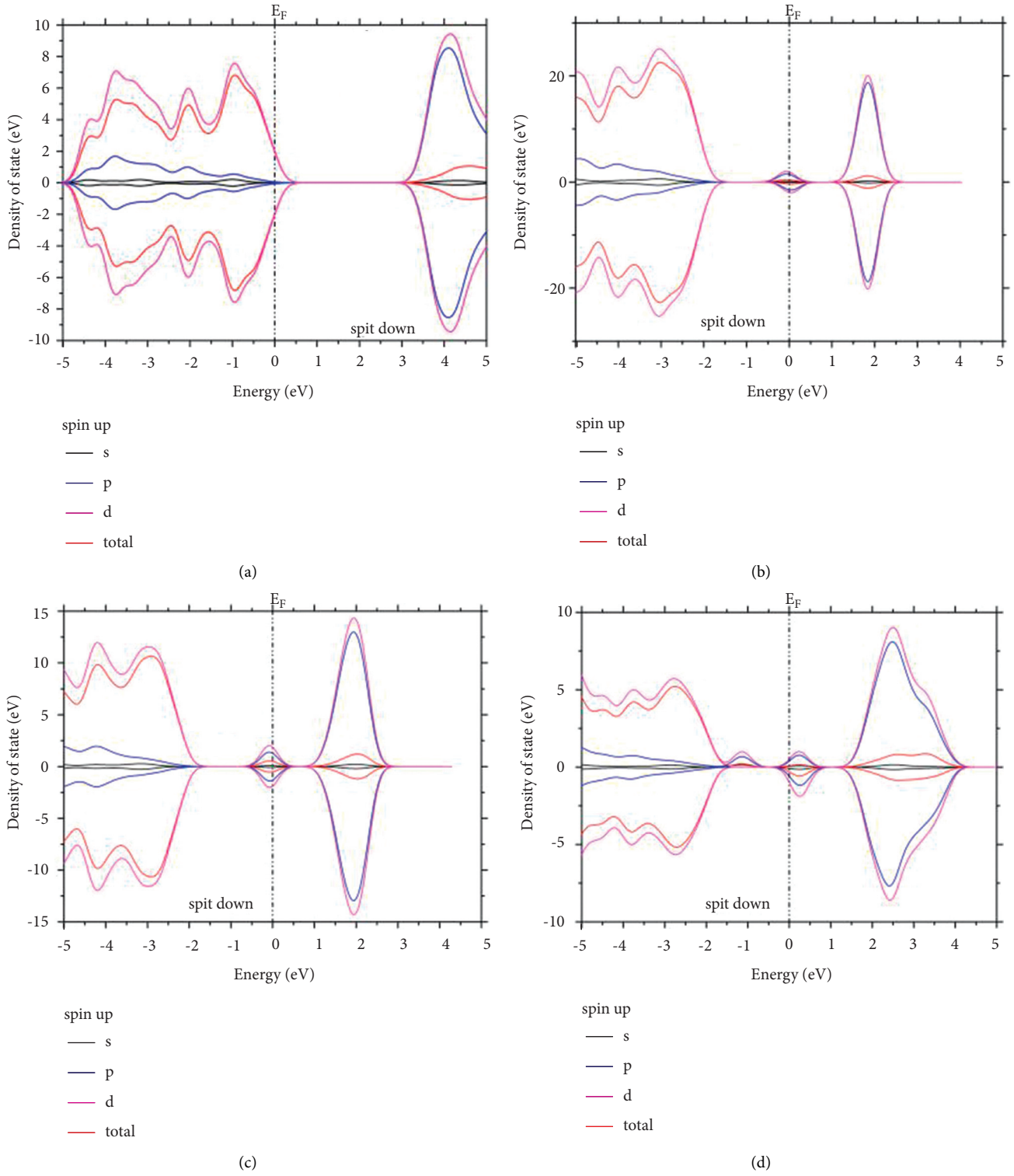

FIGURE 12: Spin density of states near the Fermi level for anatase TiO_2 with oxygen defect contents of 0% (a), 3.125% (b), 6.25% (c), and 12.5% (d).

found with nonhorizontal ordinate symmetry for the spin density of states curve near 0.2 eV. They are formed by the oxygen defect levels as shown in Figure 13(d), and this is the result of the O p state electron polarization in these areas. No visible polarization is found for the O s state electrons. It is true that the O p state electrons should be partially responsible for the local spin polarization for the anatase TiO_2 with an oxygen defect content of 12.5%.

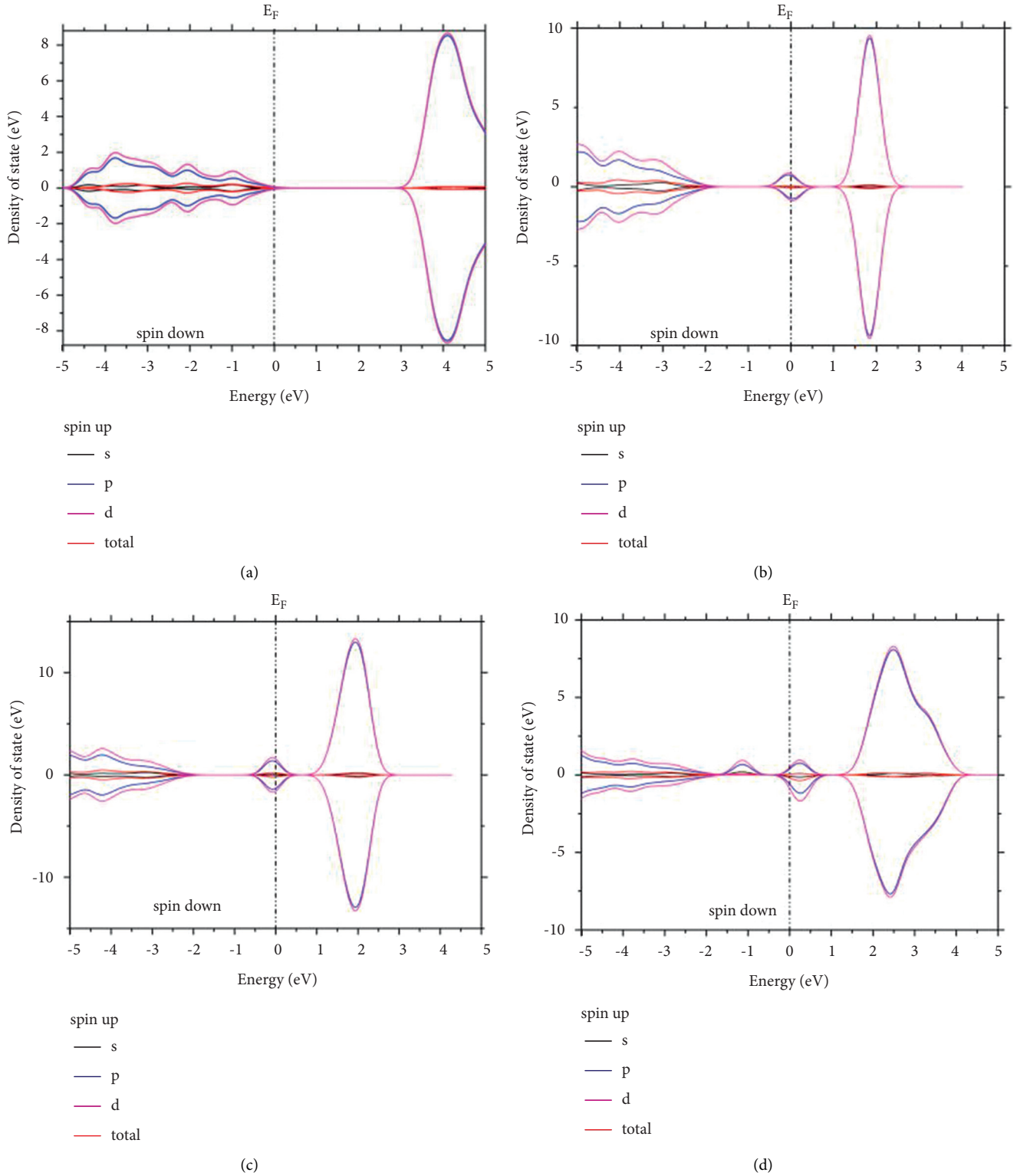

FIGURE 13: Spin density of states near the Fermi level of Ti for anatase TiO_2 with oxygen defect contents of 0% (a), 3.125% (b), 6.25% (c), and 12.5% (d).

3.5. Magnetism. Table 2 shows the deduced magnetism state for anatase TiO_2 with oxygen defect contents of 0%, 3.125%, 6.25%, and 12.5%. The results analyzed show that the ground state of TiO_2 without oxygen defect is weak paramagnetic. The anatase TiO_2 with oxygen defect contents of 3.125%, 6.25%, and 12.5% show antiferromagnetic character. Transitions from paramagnetic to antiferromagnetic are found. As discussed above, for the TiO_2 with an oxygen

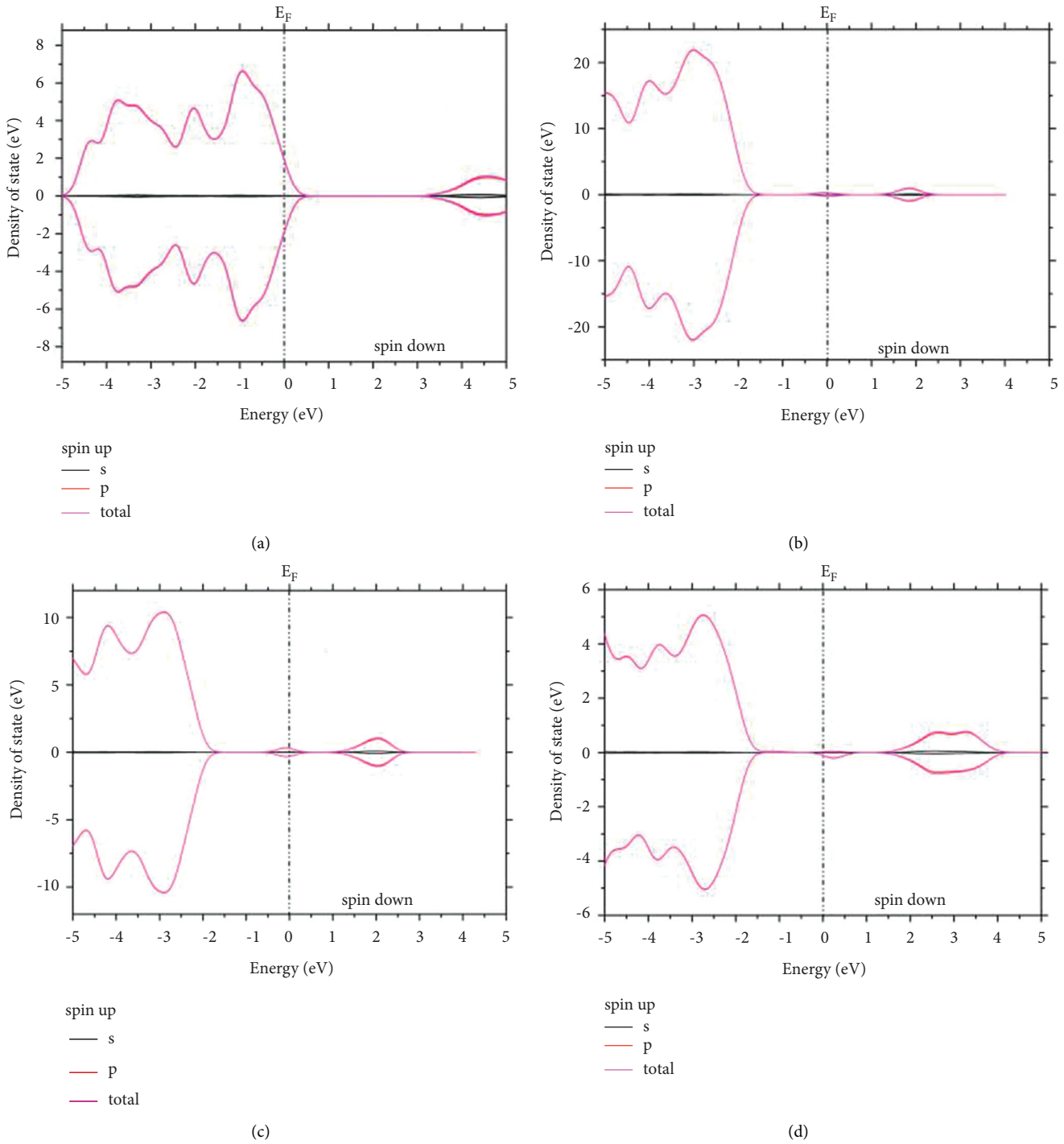

FIGURE 14: Spin density of states near the Fermi level of O for anatase TiO_2 with oxygen defect contents of 0% (a), 3.125% (b), 6.25% (c), and 12.5% (d).

defect content of 12.5%, the Ti d state electrons spin-polarized at −1.1 eV and 0.2 eV, and the O p state electrons spin-polarized at 0.2 eV. It is demonstrated that the total spin up density and the total spin down density have been compensated; thereafter, the system shows antiferromagnetic character [24].

4. Conclusions

In conclusion, the stability, geometry, microstructure, and specie combination together with the electronic states of the tetragonal anatase TiO_2 with oxygen defect contents of 0%, 3.125%, 6.25%, and 12.5% have been intensively

studied within the framework of the density functional theory calculational and analyzing method. The systems with oxygen defect have higher total energy than intrinsic TiO_2, and they are not as stable as the intrinsic TiO_2. The formation enthalpies E_f for the TiO_2 systems are −7.5122 eV, −7.4788 eV, −7.1619 eV, and −6.8003 eV. The oxygen defect gets harder to be formed. The compound with the most oxygen defect has the largest formation enthalpy; it is hardest to form. The order of magnitude for oxygen defect formation energy is approximately 10 eV, and the oxygen defect formation energy value tends to be larger for a higher defect content. The primitive cell of anatase TiO_2 shows spatial expansion when oxygen defect occurs and the strain and stress should be induced for the anatase TiO_2. The bonds within the TiO_6 polyhedron are different for the intrinsic TiO_2, and it is not geometrically symmetrical. The bond length fluctuations induced by oxygen defect are in good agreement with the lattice constants. There are two kinds of bonds within TiO_2. When there are oxygen defects, the bond strengths within the polyhedron show distinct diversity.

There are five main bands for all anatase TiO_2. All bands moved down to the low energy region and two impurity energy band levels emerged for the anatase TiO_2 with oxygen defect. The intrinsic TiO_2 belongs to the semiconductor with an indirect energy gap of 3.085 eV. The narrowest energy band gap is decreased from 3.085 eV to 1.165 eV, 1.0015 eV, and 0.43 eV for the anatase TiO_2 with oxygen defect. The energy potential for carrier to transit is indeed reduced. There are generally 7 peaks for the spin density of states curve for the intrinsic TiO_2, corresponding to its 5 bands. For the anatase TiO_2 with an oxygen defect content of 12.5%, the spin density of states curves are not horizontal ordinate symmetrical at −1.12 eV and 0.31 eV, and obvious local spin polarization is detected. The nonhorizontal ordinate symmetry is formed by oxygen defect energy levels. This is the result of the Ti d and O p state electron polarization in these areas. Transitions from weak paramagnetic to antiferromagnetic is found for the anatase TiO_2 with oxygen defect.

Data Availability

The data used to support the findings of this study are all included within the manuscript. They can also be obtained on request to the authors.

Conflicts of Interest

The authors declare that there are no conflicts of interest.

Acknowledgments

This work was supported by the National Natural Science Foundation of China under Grant nos. 21906139 and 51771003 and the Open Program of Henan Key Laboratory of Biological Psychiatry under Grant no. ZDSYS2020004. Individuals as well as organizations that contributed to this work are all acknowledged.

References

[1] W. R. Shen, W. K. Zhao, and F. He, *Progress in Chemistry*, vol. 10, p. 349, 1998.

[2] C. Z. Fan, J. P. Xiao, and Y. W. Ding, *Chinese Science Bulletin*, vol. 46, p. 365, 2001.

[3] L. T. Anh, A. K. Rai, T. V. Thi et al., "Improving the electrochemical performance of anatase titanium dioxide by vanadium doping as an anode material for lithium-ion batteries," *Journal of Power Sources*, vol. 243, pp. 891–898, 2013.

[4] X. P. Li, B. K. Xu, and G. F. Liu, *Journal of Functional Materials*, vol. 30, p. 242, 1999.

[5] Q. Wang, C. Chen, W. Ma, H. Zhu, and J. Zhao, "Pivotal role of fluorine in tuning band structure and visible-light photocatalytic activity of nitrogen-doped TiO2," *Chemistry - A European Journal*, vol. 15, no. 19, pp. 4765–4769, 2009.

[6] R. Alvarez Roca, F. Guerrero, J. A. Eiras, and J. D. S. Guerra, "Structural and electrical properties of Li-doped TiO2 rutile ceramics," *Ceramics International*, vol. 41, no. 5, pp. 6281–6285, 2015.

[7] C. McManamon, J. O'Connell, P. Delaney, S. Rasappa, J. D. Holmes, and M. A. Morris, "A facile route to synthesis of S-doped TiO2 nanoparticles for photocatalytic activity," *Journal of Molecular Catalysis A: Chemical:Chemical*, vol. 406, pp. 51–57, 2015.

[8] P. Jiang, W. Xiang, J. Kuang, W. Liu, and W. Cao, "Effect of cobalt doping on the electronic, optical and photocatalytic properties of TiO2," *Solid State Sciences*, vol. 46, pp. 27–32, 2015.

[9] R. Meng, H. Hou, X. Liu, W. Hu, J. Duan, and S. Liu, "Reassessment of the roles of Ag in TiO2 nanotubes anode material for lithium ion battery," *Ceramics International*, vol. 41, no. 8, pp. 9988–9994, 2015.

[10] Y. Gong, R. Chu, Z. Xu et al., "Electrical properties of Ta2O5-doped TiO2 varistor ceramics sintered at low-temperature," *Ceramics International*, vol. 41, no. 7, pp. 9183–9187, 2015.

[11] E. Kusmierek, *Electrocatalysis*, vol. 11, p. 555, 2021.

[12] C. Zhang, C. L. Wang, J. C. Li, K. Yang, Y. F. Zhang, and Q. Z. Wu, "Substitutional position and insulator-to-metal transition in Nb-doped SrTiO3," *Materials Chemistry and Physics*, vol. 107, no. 2-3, pp. 215–219, 2008.

[13] F. P. Zhang, J. L. Shi, J. W. Zhang, X. Y. Yang, and J. X. Zhang, "Grain alignment modulation and observed electrical transport properties of Ca3Co4O9 ceramics," *Results in Physics*, vol. 12, pp. 321–326, 2019.

[14] F. P. Zhang, Y. Sun, H. H. Wang, G. L. Zhang, G. Q. Qin, and J. X. Zhang, "Regulated microarchitecture, spin polarization state, and observed charge transfers for cerium boride CeB6 under electrical Field," *Materials Today Communications*, vol. 26, Article ID 101877, 2021.

[15] Y.-Q. Zhao, L.-J. Wu, B. Liu, L.-Z. Wang, P.-B. He, and M.-Q. Cai, "Tuning superior solar cell performance of carrier mobility and absorption in perovskite CH 3 NH 3 GeCl 3: a density functional calculations," *Journal of Power Sources*, vol. 313, pp. 96–103, 2016.

[16] Q.-K. Hu, S.-H. Qin, Q.-H. Wu et al., "First-principles calculations of stabilities and physical properties of ternary niobium borocarbides and tantalum borocarbides," *Acta Physica Sinica*, vol. 69, no. 11, Article ID 116201, 2020.

[17] Z. Y. Liu, B. Sun, X. Y. Liu et al., "15% efficient carbon based planar-heterojunction perovskite solar cells using a TiO2/SnO2 bilayer as the electron transport layer," *Journal of Materials Chemistry A*, vol. 6, p. 7409, 2018.

[18] X. Y. Yu, F. S. Li, C. S. Huang, H. Fang, and Z. H. Xu, "Anisotropic electronic structure and geometry of CaMnO3 perovskite with oxygen nonstoichiometry," *Journal of Materials Research and Technology*, vol. 9, no. 3, pp. 6595–6601, 2020.

[19] L. Bao, F. Yang, D. Cheng et al., "Modified electronic structure of Ta2O5 via surface decorated with Ta3B2 nanodots for enhanced photocatalytic activity," *Applied Surface Science*, vol. 513, Article ID 145767, 2020.

[20] A. V. Bakulin, L. S. Chumakova, and S. E. Kulkova, "Study of the diffusion properties of oxygen in TiO2," *Journal of Experimental and Theoretical Physics*, vol. 133, no. 2, pp. 169–174, 2021.

[21] K. C. L. Bauerfeind, J. Laun, M. Frisch, R. Kraehnert, and T. Bredow, "Metal substitution in rutile TiO2: segregation energy and conductivity," *Journal of Electronic Materials*, vol. 51, no. 2, pp. 609–620, 2022.

[22] P. D. Murzin, A. A. Murashkina, A. V. Emeline, and D. W. Bahnemann, "Effect of Sc3+/V5+ Co-doping on photocatalytic activity of TiO2," *Topics in Catalysis*, vol. 64, no. 13–16, pp. 817–823, 2021.

[23] A. Soussi, A. Ait Hssi, M. Boujnah et al., "Electronic and optical properties of TiO2 thin films: combined experimental and theoretical study," *Journal of Electronic Materials*, vol. 50, no. 8, pp. 4497–4510, 2021.

[24] K. Othmen, M. Abdelkader, and L. Tarek, "Theoretical and experimental investigation of the electronic, optical, electric, and elastic properties of Zn-doped anatase TiO2 for photocatalytic applications," *Appl. Phys. A-Mater*, vol. 127, p. 1, 2021.